Cavitation Characteristics during Startup Process of a Condensate Pump with Splitter Blades

C. Kang[1†], C. Lu[1], K. G. Seah[1] and W. Zhang[2]

[1]*School of Energy and Power Engineering, Jiangsu University, Zhenjiang 212013, China*
[2]*Shanghai Marine Equipment Research Institute, Shanghai 200031, China*

[†]*Corresponding Author Email: kangcan@ujs.edu.cn*

ABSTRACT

The present study aims to describe characteristics of cavitation during the startup process of a condensate pump. The pump is featured by an impeller equipped with five splitter blades. A computational fluid dynamics (CFD) work was conducted to plumb the evolution of cavitation in the pump. Effect of the volumetric flow rate on instantaneous cavitation patterns as the rotational speed of the pump increased was analyzed. The results show that high resistance to cavitation of the pump depends greatly on large area of the impeller eye, which is related to the deployment of the splitter blades. The splitter blades are insignificantly affected by cavitation. During the startup process, both the pump head and the pump efficiency vary drastically, which is insensitive to the flow rate. At a net positive suction head (NPSH) of 2.0 m, high flow rates are responsible for intensified cavitation. High volume fraction of cavitation arises near the inlet of long blades. As the rotational speed increases, the evolution of cavitation is featured by intermittency and diversified cavity patterns. Furthermore, the sum of the volume fraction of cavitation fluctuates with continuously increasing rotational speed.

Keywords: Cavitation; Condensate pump; Startup; Flow rate; Net positive suction head.

NOMENCLATURE

E_V	total volume fraction of cavitation	q_V	volumetric flowrate
H	pump head	q_{V0}	rated volumetric flow rate
NPSH	Net Positive Suction Head	t	time
$NPSH_c$	Critical Net Positive Suction Head	η	pump efficiency
n	rotational speed of the impeller		

1. INTRODUCTION

Cavitation is a phase-change phenomenon that occurs in a liquid as local pressure is decreased to be lower than a threshold value (Al-Arabi *et al*. 2011). The inception of cavitation is featured by rapid expansion of cavitation nuclei, and visible cavitation bubbles are thereby produced. These bubbles will travel with the mainstream. Arriving at some positions with relatively high pressure, cavitation bubbles collapse due to imbalance of pressure between the inner and outer sides of the bubble. Collapse of cavitation bubbles incurs noise, vibration of the mechanical device or even cavitation erosion of hydraulic components (Chudina 2003; Liu *et al*. 2020). The consequence

of cavitation in fluid machinery can be disastrous (Adamkowski *et al*. 2016). Complex mechanism of cavitation is closely related to transient phase-change characteristics and the diversity of the factors influencing the evolution of cavitation (Azizi *et al*. 2017).

The condensate pump plays an important role in various thermal systems (Ibrahim and Attia, 2015). For such a pump, the risk of cavitation is high since gas may be entrained in the liquid entering the pump. Delivery of the liquid containing cavitation bubbles poses a threat to stable operation of the equipment downstream of the condensate pump. For the impeller pump, one of the most distinct features is the interaction between liquid and the rotating impeller, which inevitably influences the development of cavitation in the flow passage of the

pump (Mousmoulis *et al.* 2019). Effects of the operational parameters of the pump on cavitation have been investigated by Fu *et al.* (2016), and explicit variation tendencies were revealed. Generally, at high cavitation intensity, the flow passage of the impeller is dominated by swarms of cavitation bubbles. In this case, the performance degradation of the pump is predictable.

Fundamental investigations of cavitation have been performed in two major aspects, namely cavitation visualization and the detection of the signals emitted by cavitation bubble collapse (Binama *et al.* 2016). Cavitation zone is attached to the suction side of the blade, which is typical for the centrifugal pump. Previous studies put emphasis on normal operation of the pump; however, the startup process is also critical for the pump. Instability nurtured during such a process can be amplified, and subsequent operation of the pump will be affected. The startup process is characterized by time-varying rotational speed (Zhang *et al.* 2014), and the pump head varies accordingly (Lefebvre and Barker 1995). Essentially, transient flow phenomena arising during the startup process of the pump are significantly different from those associated with the stable operation. As cavitation occurs during the startup process of the pump, the inter-phase interaction is complicated by inherently unstable nature of cavitation and the liquid flow driven by the rotating impeller. Thus far, studies in this respect have seldom been reported.

Effect of cavitation on operation of the pump can be described based on test data. However, measurement of instantaneous pump head and pump efficiency is not easy since attainable temporal resolution of available instrument is fairly low. Fundamentally, experimental work on cavitation has been conducted using the high-speed photography or high-sensitivity pressure transducers (McKee *et al.* 2015; Černetič and Čudina 2011). In these cases, the obtained images or data provide a sound support to the design of hydraulic components of the pump. Feasibility of performing these experimental studies depends on the pump structure, which should allow for proper configuration of the light source and the high-speed camera, or deployment of pressure sensors.

The computational fluid dynamics (CFD) technique helps to deepen the understanding of cavitating flows in the pump (Kang *et al.* 2017a). Based on numerical results, unsteady flows in a hydraulic turbine were described in Wu *et al.* (2012), which demonstrated the ability of CFD in predicting flow phenomena associated with the rotating impeller. Advanced CFD techniques such as large eddy simulation (LES) and detached eddy simulation (DES) have been applied in this aspect as well. At present, the combination of Reynolds averaged Navier Stokes (RANS) equations and the turbulence model is still a predominant approach. Moreover, several cavitation models have been developed and validated through experimental results (Pouffary *et al.* 2008). A CFD simulation of cavitation for an impeller pump enables building a relationship between cavity patterns, velocity or pressure distributions, and performance indicators of the pump.

The present study aims to describe cavitation characteristics of a condensate pump during its startup process. Both experimental and numerical techniques were applied. Operational and cavitation performance of the pump was measured based on a closed test loop. A numerical scheme was designed and validated through experimental results. Distributions of flow parameters and cavities in the pump were simulated and analyzed. Furthermore, at high flow rates, the startup processes of the pump were simulated, and cavitation was described through the volume fraction of cavitation. A comprehensive comparison was performed between the results obtained at different flow rates. The conclusions help to expand the knowledge of the cavitation associated with the startup process of the impeller pump.

2. DESCRIPTION OF THE CONDENSATE PUMP

The pump considered, as shown in Fig. 1, is a vertically-installed centrifugal pump, which is featured by five long and five splitter blades. With such an impeller structure, the blockage effect at the blade inlet is mitigated, and the flow divergence
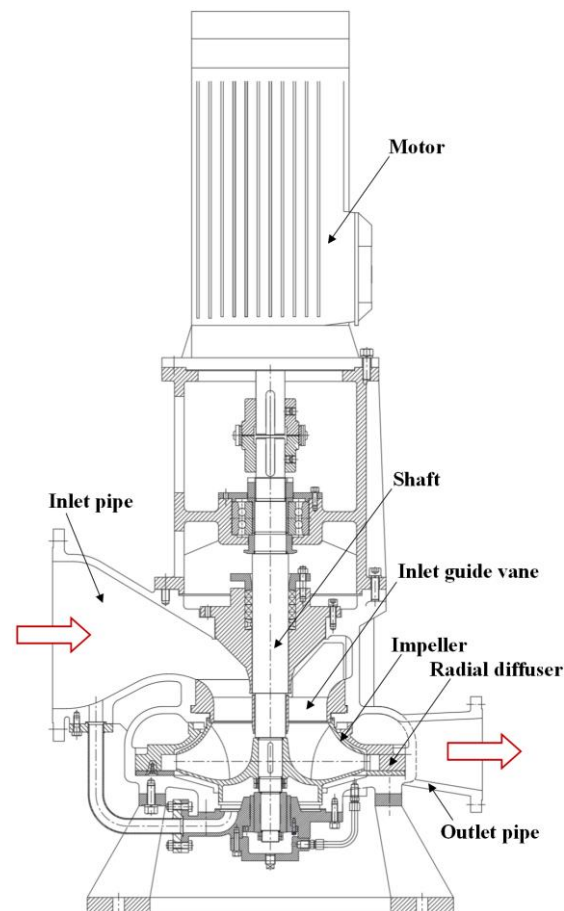
Fig. 1. Schematic view of the pump structure.

Table 1. Main parameters of the pump

Parameters	Value
Design flow rate (m³/h)	227
Pump head (m)	28
Rotational speed (rpm)	1230
Required net positive suction head (m)	1.0
Impeller eye diameter (mm)	215
Impeller outer diameter (mm)	350
Impeller outlet width (mm)	29
Blade wrap angle for long blade (°)	112
Blade wrap angle for short blade (°)	52

at the downstream part of the blade passage is suppressed as well (Guo *et al*. 2015; Abo Elyamin *et al*. 2019). However, the pump efficiency at the rated flow rate is slightly lower than that of the pump equipped with equal-length blades. Main parameters of the pump are listed in Table 1. Pure water of 20°C flows into the impeller in an overall downward direction after passing through an inlet guide vane, which is responsible for alleviating pre-swirling of the incoming liquid and restricting lateral motion of liquid. Energy is then delivered to the liquid medium via the rotating blades. A radial diffuser with six flow passages is mounted around the impeller. Such a stationary component connects the impeller with the pump casing, and stabilizes the liquid medium discharged from the impeller. The liquid medium is expelled from the radial diffuser and then enters the annular chamber enclosed by the pumping casing. Eventually, liquid is discharged from the pump through the outlet pipe along a horizontal direction.

Experiment of the pump furnishes a direct and objective evaluation of the performance of the pump. Nevertheless, for the cavitation experiment of the pump shown in Fig. 1., it can only be conducted through measuring the net positive suction head (*NPSH*). More specifically, observation of the cavitation pattern in the pump is impractical even as a transparent pump model is fabricated. In this case, the CFD technique can be used to investigate cavitating flows in the pump and the relationship between cavitation and the pump

performance. Moreover, the obtained numerical and experimental results can be comprehensively analyzed to further the understanding of the cavitation performance of the pump.

3. EXPERIMENTAL AND NUMERICAL SETUP

3.1 Experimental Rig

The experimental rig was constructed based on a closed loop, as schematically shown in Fig. 2. Pure water of 20°C served as the liquid medium. In parallel with practical application, the pump is vertically installed. Both the test loop and the instruments employed conform to the standard ISO 9906:2012. The specified uncertainties for the electromagnetic flow meter, the pressure transmitters and the pocket laser tachometer are ±0.5%, ±0.25% and ±0.01% (relative to the readout), respectively. For the experimental uncertainty, it is composed of random and systematic uncertainties. For the performance test under no-cavitation conditions, the overall uncertainties for the flow rate, the rotational speed, the input torque and the pump head are ±2.8%, ±1.8%, ±2.5% and ±3.2%, respectively. For the cavitation experiment, the vacuum degree in the tank was adjusted through the vacuum pump. At each flow rate, available NPSH was reduced progressively until the relative drop of the pump head reached 3%. The overall uncertainty in measurement of critical NPSH is less than ±6%. Measurement at each flow rate was repeated five times to ensure repeatable results were obtained.

In the loop, cavitation bubbles might be circulated with the main stream since they cannot be completely annihilated. Therefore, after each experiment at a volumetric flow rate, the tank was emptied and refilled, and the liquid level was kept the same for all the cases. Before and after each experiment, the liquid temperature was measured to calculate the saturation vapor pressure. Since the tank is spacious enough, the fluctuation of liquid temperature during the experiment is less than 4°C.
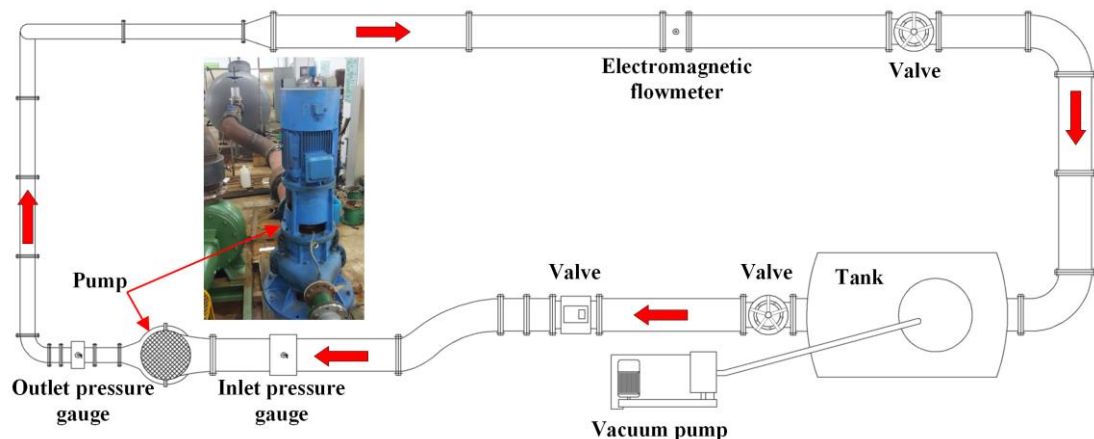
Fig. 2. Experimental rig.
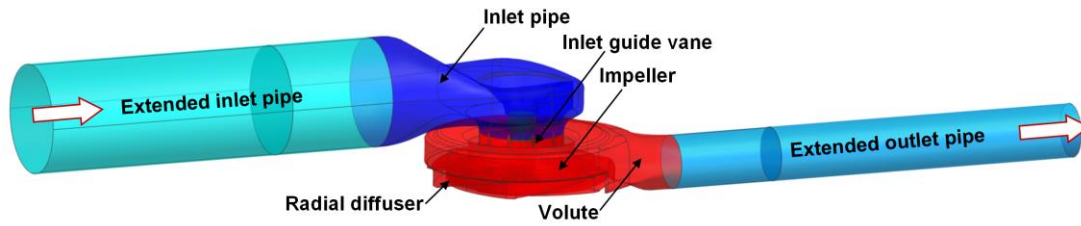
Fig. 3. Three-dimensional computational domain.

3.2 Computational Model of the Pump

For the numerical work, a three-dimensional computational domain, which is consistent with the flow passage of the pump, was built. The whole domain consists of several subdomains, as marked in Fig. 3. This allows for applying different grid schemes to discretize individual subdomains. Here, the extended inlet and outlet straight pipe segments ensure full development of inlet flow and no reverse flow at the outlet. The inlet and outlet diameters of the computational domain shown in Fig. 6 are 300 mm and 150 mm, respectively. Two rotor-stator interfaces were specified in the domain, one connected the inlet guide vane and the impeller and the other for the impeller and the radial diffuser. The technique of the transient rotor-stator interface was adopted. All interaction effects between components that were in relative motion to each other were thereby considered. The interface position was updated at each time step, as relative position of the grids on each side of the interface changed.

3.3 Numerical Models

Unsteady Reynolds-averaged Navier-Stokes (URANS) equations were used as the equations governing the motion of the viscous liquid medium in the condensate pump. The Re-Normalisation group (RNG) k-ε turbulence model was selected to attain the closure of the governing equations. With a cavitation model, the inception of cavitation and the interaction between cavitation bubbles and surrounding liquid are addressed (Singhal *et al.* 2002). Here, the Schnerr-Sauer model based on the Rayleigh-Plesset equation was used. Details of the numerical strategy can be found in Kang *et al.* (2017b). In the present study, numerical simulations were implemented using the commercial CFD code ANSYS CFX.

3.4 Boundary and Initial Conditions

The pressure inlet boundary condition was specified at the inlet of the computational domain, and available *NPSH* can be adjusted. At the outlet of the computational domain, the velocity boundary condition was set to ensure certain flow rate. No-slip boundary conditions were set for all solid walls wetted by the liquid medium. In parallel with the real product, the surface roughness of the blade surfaces was set to 25 μm. For other surfaces, the surface roughness was set to 12.5 μm. Flows in near-wall flow regions were treated with scalable wall functions. Thereby, spurious solutions incurred by small y^+ values or excessive refinement of near-wall grids can be avoided.

At each flow rate, the results of steady numerical simulation were used as the initial condition for unsteady computation. The initial volume fraction of cavitation was set to 5×10^{-4} and the radius of the cavitation nuclei was identically 10^{-3} mm. The time step was set as the timespan with which the impeller rotated for 1° at the rotational speed of 1230 rpm. Accordingly, the maximum Courant number was less than 0.9. The convergence criteria of 10^{-4} was designated for each monitored quantity. A smaller timestep, namely 0.5°, was responsible for insignificant improvement of accuracy of the pump head or the pump efficiency.

3.5 Grid Independence Examination

To eliminate the effect of grid number on the numerical results, a grid independence examination was conducted and five grid schemes were designed. Apart from the pump head and the pump efficiency, local pressures along the axis of the outlet pipe of the pump were also monitored according to the approach proposed by Pei *et al.* (2020). The results show pressure fluctuations are not synchronous with variation of the pump head or the pump efficiency, and as the grid number attains a certain level, characteristic frequencies of pressure fluctuations remain nearly invariant. However, the peak and valley pressures still vary with grid number. This is related to not just grid number but also the time step selected. Therefore, the pump head and the pump efficiency were used for the grid independence examination, as shown in Fig. 4. It is seen that as total grid number exceeds
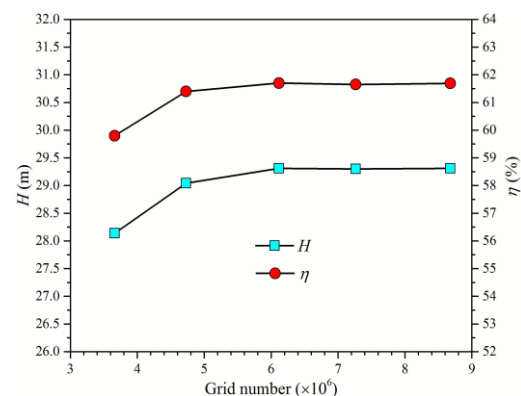
Fig. 4. Mesh independence examination.
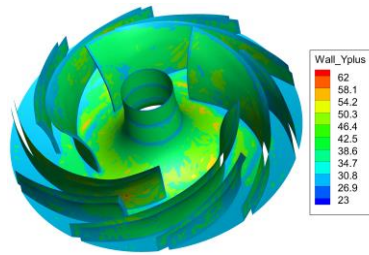
Fig. 5. Distribution of *y+* over blade surface.

620 million, the difference of the pump head between two neighboring grid schemes is less than 0.87%. In view of the computational accuracy and economy, the grid scheme with 7,264,136 unstructured grids was finally selected. Regarding this grid scheme, the maximum equiangle skewness of the grids is 0.53. Meanwhile, the obtained y^+ values range from 23 to 62, and distributions of $y+$ over the blade surface are shown in Fig. 5. In consideration of the requirements of the high Reynolds number RNG k-ε turbulence model, near-wall viscosity effect has been properly considered.

4. VALIDATION OF THE NUMERICAL SCHEME

To examine the physical validity of the numerical scheme, a comparison was implemented between numerical and experimental results, as shown in Fig. 6. For the pump head or the pump efficiency, the variation tendencies of the numerical and the experimental results are similar. Generally, numerical results are larger than their counterparts. This is related to that some practical factors could not be taken into account in numerical settings. At low flow rates, deviation of the numerically obtained pump head from the experimental data is relatively large; however, the maximum deviation is less than 6%. For the pump efficiency, since the experimental results involve mechanical, volumetric and hydraulic efficiencies, and only the hydraulic efficiency was obtained through the numerical simulation. Therefore, the numerical data is relatively high. A high validity of the numerical scheme is proved from an overall perspective.
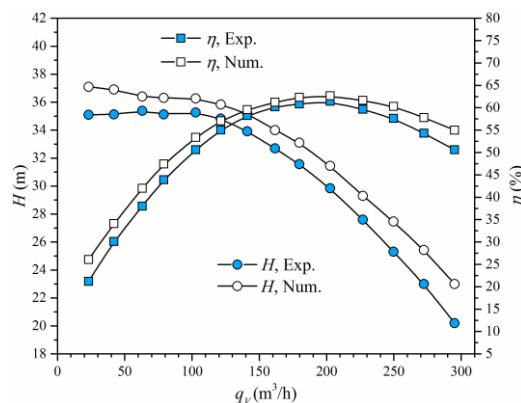
Fig. 6. Comparison of pump performance between numerical and experimental results.

A further validation was performed with an emphasis placed on the cavitation performance of the pump, and the results are plotted in Fig. 7. As q_v increases, $NPSH_c$ increases gradually, which is shared by the experimental and numerical results. After q_v exceeds 272 m³/h, $NPSH_c$ increases sharply, indicating high possibility of cavitation at high flow rates. In comparison, numerically obtained $NPSH_c$ is lower compared to corresponding experimental data, but the deviation is acceptable. The suitability of the numerical strategy in predicting cavitation performance of the pump is confirmed.
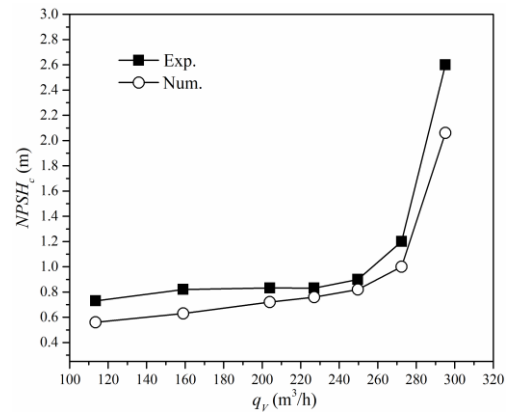
Fig. 7. Comparison of cavitation performance between numerical and experimental results.

5. FLOW CHARACTERISTICS OF THE PUMP

As the liquid medium travels from the inlet to the outlet of the pump at $q_v=q_{v0,}$ pressure increases continuously and smoothly, as shown in Fig. 8(a), indicating stable operation of the pump. In the impeller eye area, low pressure is predominant. Such a low-pressure area promotes the onset of cavitation. Meanwhile, regarding the splitter blades, they are neighbored by relatively high pressure. This demonstrates that the contribution of the splitter blades to the pump head is maintained. Furthermore, when the splitter blades are further shortened, or the impeller eye area is further enlarged, the possibility of cavitation can be further reduced. However, the pump head will decrease; in this case, the outlet diameter of the impeller may be required to enlarge to attain the same pump head. In the flow passage of the diffuser, fairly uniform distribution of high pressure is demonstrated.

The distribution of vectors of the relative velocity is shown in Fig. 8(b). In the impeller eye, a large-scale circulation is formed, as marked with zone A. The circulation directly results in hydraulic loss. Near the inlet of the splitter blades (zone B), vortices are recognizable but the vortex intensity is relatively low. Furthermore, high velocity is produced at the inlet of the diffuser and the outlet of the impeller since local flow area is minimized (zone C). Symmetry of the velocity distribution about the impeller axis is high relative to that associated with

(a) Pressure distribution

(b) Distribution of relative velocity vectors
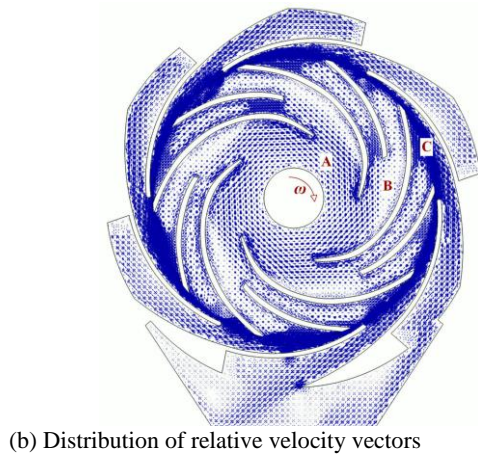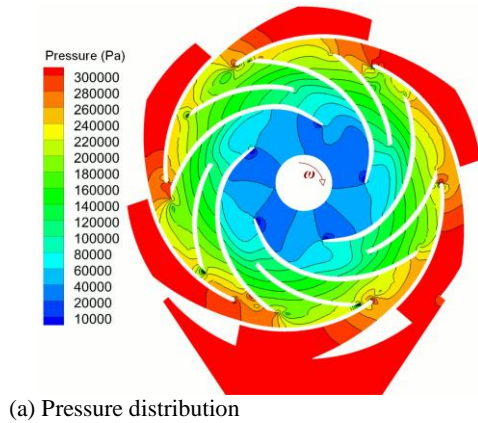
Fig. 8. Cross-sectional flow parameter distributions in the pump.

Fig. 9. Isosurfaces for volume fraction of cavitation of 0.5 at *NPSH*=2.0 m and q_V=q_{V0}.
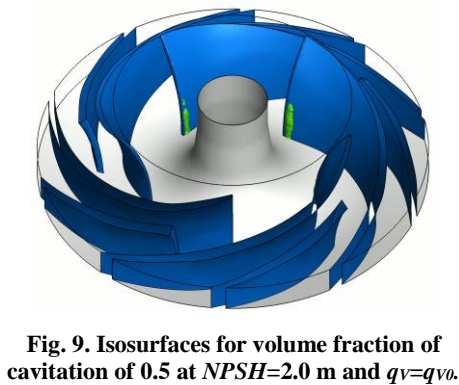
the spiral volute (Azad *et al*. 2019). On the whole, high quality of the inner flow of the pump is attained.

At q_V=q_{V0} and *NPSH*=2.0 m, slight cavitation arises in the pump, as illustrated in Fig. 9. Isosurfaces with identical volume fraction of cavitation of 0.5 are presented. It is evidenced that cavitation elements are attached to the inlet and suction side of the long blades. A joint consideration of Figs. 8(a) and 9 indicates that cavitation is inherently related to the static pressure (Zhao *et al*. 2016). Moreover, the curved surface has a significant effect on cavitation (Zhou *et al*. 2019). However, the distribution of cavitation elements is not ultimately

consistent with the pressure distribution. Furthermore, for each blade, the attached cavitation elements exhibit different patterns, and cavitation bubbles keep shedding from each blade surface and then regenerating, signifying unsteadiness nature of the development of cavitation.

Based on the variation of $NPSH_c$ with the flow rate plotted in Fig. 7, it is conceivable that the pump head is significantly influenced by the accumulation of cavitation bubbles in the flow passage. The intensity of cavitation is dependent of the flow rate of the liquid medium (Gohil and Saini 2015). High flow rates lead to intensified cavitation. In its practical application, the condensate pump considered generally operates at high flow rates. Literally, high flow rates promote the inception of cavitation. In present study, at q_V=1.1q_{V0}, 1.2q_{V0} and 1.3q_{V0}, the distributions of pressure in the flow passage of the impeller were constructed based on the numerical results and are presented in Fig. 10.

(a) q_V=1.1q_{V0}

(b) q_V=1.2q_{V0}

(c) q_V=1.3q_{V0}
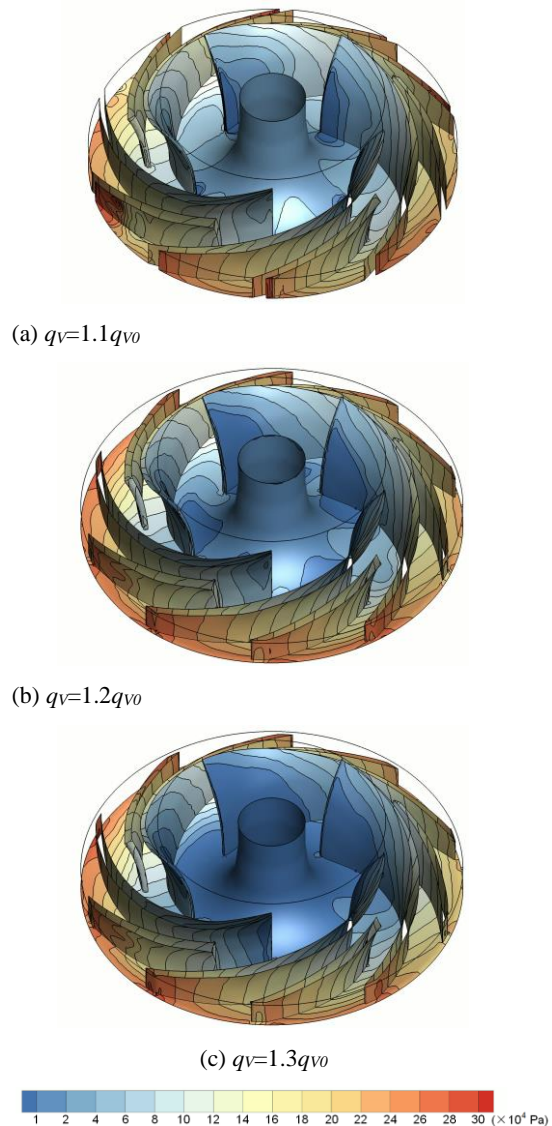
Fig. 10. Pressure distributions at different *NPSH*s.

At the three flow rates, an *NPSH* value of 2.0 m is associated with remarkable difference in cavitation performance, as implied in Fig. 7. Therefore, such an *NPSH* value was selected to enable a comprehensive comparison between the startup processes at the three flow rates.

6. CAVITATION DURING STARTUP PROCESS

6.1 Variation of Rotational Speed during Startup Process

In parallel with practical situation, the startup process of the pump is finished within 12 s. Accordingly, the rotational speed of the impeller, *n*, is required to increase from 0 to 1230 rpm during such a period, as indicated in Fig. 11. With available pressure sensors and flowmeters, instantaneous pump head and pump efficiency are difficult to obtain since calculation of the two operating parameters necessitates a simultaneous consideration of pressures and velocities at the points in the inlet and outlet cross sections. Here, unsteady numerical simulation was performed to capture instantaneous operational parameters of the pump. Time-dependent rotational speed was imposed onto the impeller through user defined functions, which was executed with the solver of the governing equations.
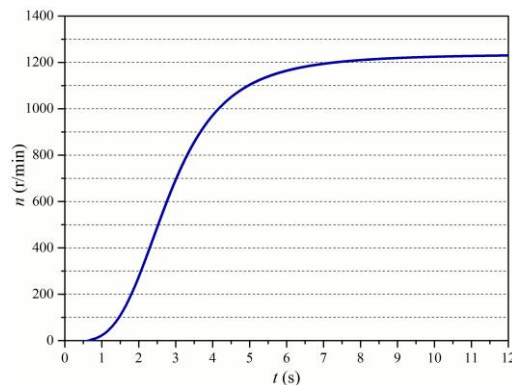
Fig. 11. Variation of rotational speed during startup process.

6.2. Startup Process at $q_V=1.1q_{V0}$

At *NPSH*=2.0 m and $q_V=1.1q_{V0}$, the pump head and the pump efficiency are plotted in Fig. 12 as functions of the startup time, *t*. Apparently, variation of the pump head is rather regular. The most distinct fluctuations occur in the initial stage of the startup process. Regarding the pump efficiency, it fluctuates as well but the fluctuation is not in exact pace with that of the pump head, signifying difference in the factors influencing the two quantities.

According to Fig. 7, cavitation occurs at *NPSH*=2.0 m and $q_V=1.1q_{V0}$. Therefore, with increasing rotational speed, fluctuations of the pump head and the pump efficiency are inevitable; meanwhile,

cavitation intensity is enhanced as well. However, based on the two curves shown in Fig. 12, adverse effect of cavitation on the performance of the pump is not explicit.
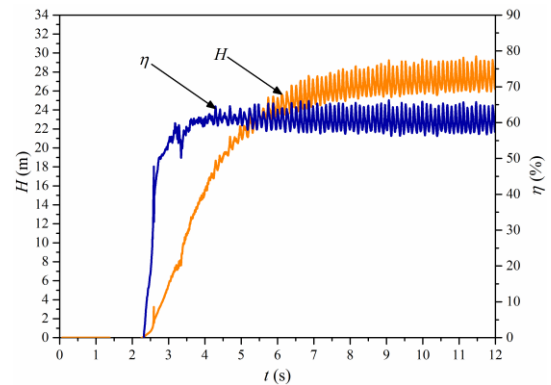
Fig. 12. Variations of pump head and pump efficiency during startup process at 1.1q_{V0}.

At $q_V=1.1q_{V0}$, the evolution of cavitation in the flow passage of the impeller during the startup process is shown in Fig. 13. Here, the volume fraction of cavitation for the isosurfaces is set to 0.1. At *t*=2.51 s, cavitation elements attached to the inlet of long blades are already remarkable. Hence, as *n* increases further, pressure in the impeller area is

(a) *t*=2.51 s   (b) *t*=2.78 s

(c) *t*=2.82 s   (d) *t*=3.04 s

(e) *t*=3.11 s   (f) *t*=3.34 s
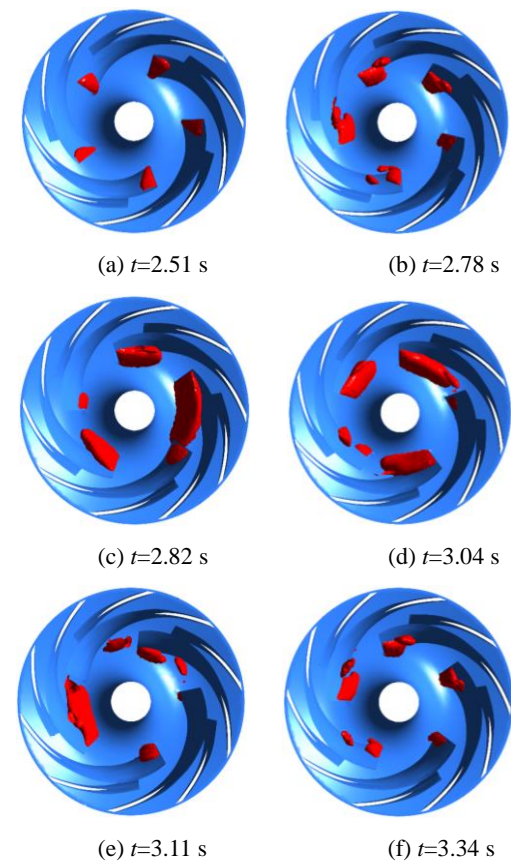
Fig. 13. Evolution of cavitation during the startup process at 1.1q_{V0}.

reduced, resulting in expansion of local cavitation zones. Meanwhile, cavitation bubbles exhibit concentrated patterns near the blade inlet but are sparsely distributed away from the blade. The symmetry with respect to the impeller blades is weak. Furthermore, the splitter blades are not directly impacted by cavitation bubbles. After t=3.34 s, cavitation elements remain fairly stable and further growth of the cavitation volume is suppressed.

6.3. Startup Process at q_V=1.2q_{V0}

At q_V=1.2q_{V0}, variations of H and η are plotted in Fig. 14. Relative to those shown in Fig. 11, fluctuations of the two performance indicators are considerably intensified. In an average manner, both the pump head and the pump efficiency decrease with increasing flow rate. This is in accordance with real situation of the pump.
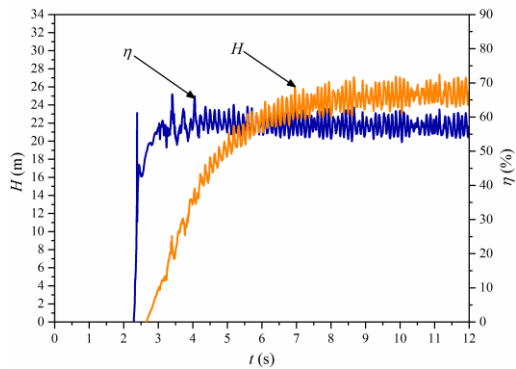
Fig. 14. Variations of pump head and pump efficiency during startup process at 1.2q_{V0}.

Actually, even as the operation of the pump arrives at a stable state, fluctuations of the rotational speed are recognizable. This inevitably leads to variations of the pump head and the pump efficiency. To ensure operational stability, variation amplitudes of n, H and η should be confined within some ranges.

Typical cavitation patterns obtained at q_V=1.2q_{V0} are shown in Fig. 15. As n increases continuously, cavitation zones at the inlet and suction side of the long blades expand remarkably. In comparison, cavitation elements with a relatively small volume are formed at the inlet of the splitter blades, as indicated in Fig. 15(a). Furthermore, intermittency is clear since the cavitation zones vanish at t=2.95 s and recur later. It is noteworthy that variation of the cavitation volume fraction is not synchronous with that of the pump head or the pump efficiency. As t increases, local cavitation zones manifest diverse profiles. Some cavitation zones are disintegrated and some elements are sparsely distributed in the impeller eye area. At t=4.49 s, cavitation zones tend to be connected in circumferential direction. Such a state exerts a threat to the throughflow of the liquid medium. Based on Figs. 15 and 13, it is evidenced that the increase in the volume fraction of cavitation with the flow rate is distinct. Meanwhile, the five splitter blades are insignificantly influenced by

cavitation, as illustrated in Fig. 15. This partially explains why the capability of the pump in alleviating cavitation is high.

(a) t=2.33 s (b) t=2.95 s

(c) t=3.10 s (d) t=4.49 s

(e) t=9.01 s (f) t=11.00 s
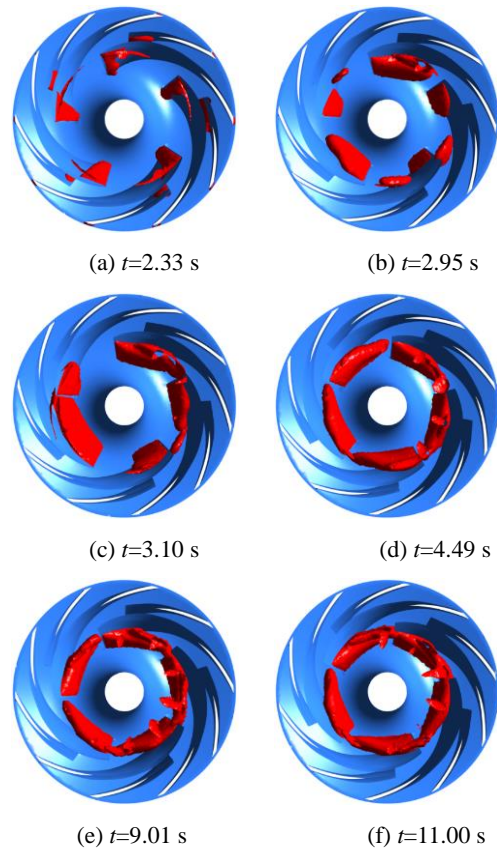
Fig. 15. Evolution of cavitation during the startup process at 1.2q_{V0}.

6.4. Startup Process at q_V=1.3q_{V0}

The startup process was simulated at q_V=1.3q_{V0} and $NPSH$=2.0 m, and the result is diagramed in Fig. 16. Relative to that shown in Fig. 14, the pump head corresponding to q_V=1.3q_{V0} fluctuates drastically during the whole startup process. Even approaching t=12 s, H and η have not been stabilized. High fluctuation amplitudes of H and η are closely related to intensified cavitation with increasing flow rate.

Under the circumstance indicated in Fig. 16, cavitation significantly influences the operation of the pump. Both the average pump head and pump efficiency obtained at q_V=1.3q_{V0} are lower than those obtained at the two lower flow rates.

As the flow rate increases from 1.2q_{V0} to 1.3q_{V0}, the relative velocity in the flow passage of the impeller is increased and the static pressure decreases accordingly. Therefore, at the same rotational speed, the volume fraction of cavitation at q_V=1.3q_{V0} is relatively high. In circumferential direction and near the inlet edges of the long blades, cavitation zones are connected, as shown in Fig. 17. In this case, cavities are even observed in the flow passages
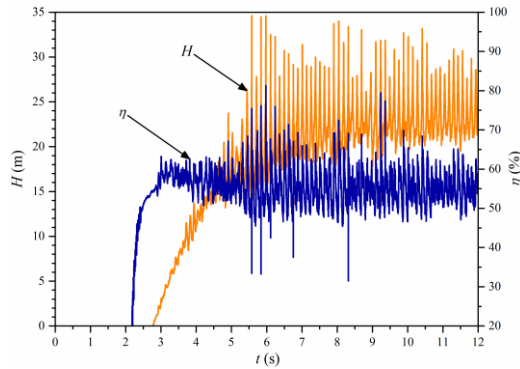
Fig. 16. Variations of pump head and pump efficiency during startup process at 1.3q_{V0}.

enclosed by the inlet guide vane. This indicates an instantaneous state of the coexistence of cavities and liquid. Furthermore, highly frequent generation of cavities will block the flow passage designed for transporting liquid. For the splitter blades, no attached cavity is identifiable. Nevertheless, as cavitation bubbles travel with the liquid flow, the interaction between the splitter blades and cavitation bubbles is inevitable. Regarding where cavitation bubbles will ultimately collapse, it depends greatly on local liquid flow.

(a) t=2.33 s (b) t=2.95 s

(c) t=3.10 s (d) t=4.49 s

(e) t=9.01 s (f) t=11.00 s
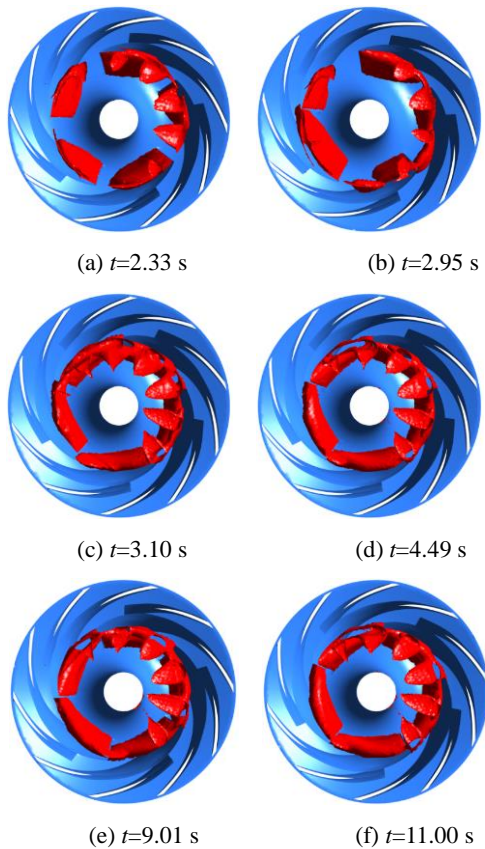
Fig. 17. Evolution of cavitation during the startup process at 1.3q_{V0}.

6.5. Total Volume Fraction of Cavitation

At the three flow rates, time-dependent total volume fraction of cavitation, E_V, was calculated and diagramed in Fig. 18. It is seen that the total volume fractions of cavitation at the end of the startup process are considerably different. The increase in the flow rate causes an increase of cavitation intensity. Meanwhile, as n increases, E_V fluctuates, as is shared by the cases of q_V=1.2q_{V0} and 1.3q_{V0}. This demonstrates an intermittency of the evolution of cavitation. At q_V=1.1q_{V0}, the development of cavitation is apparently suppressed, which is evidenced in Fig. 18.
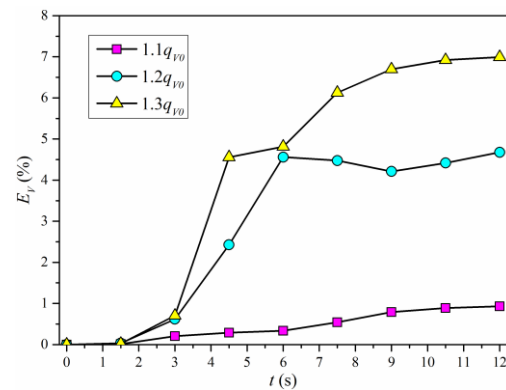
Fig. 18. Total volume fraction of cavitation at different flow rates.

7. CONCLUSIONS

(1) A high ability of mitigating cavitation is demonstrated for the condensate pump equipped with splitter blades. This is largely attributed to the spacious impeller eye zone. Although low pressure is caused in such a zone, its adverse effect on the splitter blades is limited.

(2) The pump head and the pump efficiency vary explicitly during the startup process. As the flow rate increases, the fluctuations of the two quantities are intensified. At the highest flow rate considered, cavitation zones tend to be connected in circumferential direction, and the pump performance is degraded.

(3) During the startup process, cavitation zones are not symmetrically distributed over each blade. Coexistence of attached cavities and sparsely distributed cavitation elements is demonstrated. Variation of the volume fraction of cavitation is not monotonous as the rotation of the impeller is accelerated.

ACKNOWLEDGEMENTS

REFERENCES

Abo Elyamin, G. R. H., M. A. Bassily, K. Y. Khalil and M. Sh. Gomaa (2019). Effect of impeller blades number on the performance of a centrifugal pump. *Alexandria Engineering Journal* 58(1), 39–48.

Adamkowski, A., A. Henke and M. Lewandowski (2016). Resonance of torsional vibrations of centrifugal pump shafts due to cavitation erosion of pump impellers, *Engineering Failure Analysis* 70, 56–72.

Al-Arabi, A. A. B., S. M. A. Selim, R. Saidur, S. N. Kazi and G. G. Duffy (2011). Detection of cavitation in centrifugal pumps. *Australian Journal of Basic and Applied Sciences* 5, 1260–1267.

Azad, S., H. Lotfi and A. Riasi (2019). The effects of viscoelastic fluid on the cavitation inception and development within a centrifugal pump: An experimental study. *International Communications in Heat and Mass Transfer* 107, 106–113.

Azizi, R., B. Attaran, A. Hajnayeb, A. Ghanbarzadeh and M. Changizian (2017). Improving accuracy of cavitation severity detection in centrifugal pumps using a hybrid feature selection technique. *Measurement* 108, 9–17.

Binama, M., A. Muhirwa and E. Bisengimana (2016). Cavitation effects in centrifugal pumps-A review. *International Journal of Engineering Research and Applications* 6, 52–63.

Černetič, J. and M. Čudina (2011). Estimating uncertainty of measurements for cavitation detection in a centrifugal pump, *Measurement* 44, 1293–1299.

Chudina, M. (2003). Noise as an indicator of cavitation in a centrifugal pump. *Acoustical Physics* 49(4), 463–474.

Fu, Q., F. Zhang, R. S. Zhu and B. He (2016). A systematic investigation on flow characteristics of impeller passage in a nuclear centrifugal pump under cavitation state, *Annals of Nuclear Energy* 97, 190–197.

Gohil, P. P. and R. P. Saini (2015). Effect of temperature, suction head and flow velocity on cavitation in a Francis turbine of small hydro power plant, *Energy* 93, 613–624.

Guo, X. M., Z. C. Zhu, B. L. Cui and Y. Li (2015). Effects of the short blade locations on the anti-cavitation performance of the splitter-bladed inducer and the pump, *Chinese Journal of Chemical Engineering* 23, 1095–1101.

Ibrahim, S. M. A. and S. I. Attia (2015). The influence of condenser cooling seawater fouling on the thermal performance of a nuclear power plant. *Annals of Nuclear Energy* 76, 421–430.

Kang, C., G. F. Zhang, B. Li, Y. H. Feng and Z. G. Zhang (2017a). Virtual reconstruction and performance assessment of an eroded centrifugal pump impeller. *Proceedings of the Institution of Mechanical Engineers, Part C: Journal of Mechanical Engineering Science* 231(12), 2340–2348.

Kang, C. N. Mao, W. B. Zhang and Y. P. Gu (2017b). The influence of blade configuration on cavitation performance of a condensate pump. *Annals of Nuclear Energy* 110, 789-797.

Lefebvre, P. J. and W. P. Barker (1995). Centrifugal pump performance during transient operation. *ASME Journal of Fluid Engineering-Transactions of the ASME* 117(2), 123–128.

Liu, H. X., C. Kang and H. Soyama (2020). Experimental study of the influence of test chamber dimensions on aggressive intensity of the cavitating jet. *Journal of Test and Evaluation* 48(5), 3588–3601.

McKee, K., G. L. Forbes, I. Mazhar, R. Entwistle, M. Hodkiewicz and I. Howard (2015). A vibration cavitation sensitivity parameter based on spectral and statistical methods. *Expert Systems with Applications* 42, 67–78.

Mousmoulis, G., N. Karlsen-Davies, G. Aggidis, I. Anagnostopoulos and D. Papantonis (2019). Experimental analysis of cavitation in a centrifugal pump using acoustic emission, vibration measurements and flow visualization. *European Journal of Mechanics B-fluids* 75, 300–311.

Pei, J., M. K. Osman, W. Wang, J. Yuan, T. Yin and D. Appiah (2020). Unsteady flow characteristics and cavitation prediction in the double-suction centrifugal pump using a novel approach. *Proceedings of the Institution of Mechanical Engineers, Part A: Journal of Power and Energy* 234, 283–299.

Pouffary, B., R. F. Patella, J. L. Reboud and P. A. Lambert (2008). Numerical simulation of 3D cavitating flows: Analysis of cavitation head drop in turbomachinery. *Journal of Fluids Engineering-Transactions of the ASME* 130, 061301.

Singhal, A. K., M. M. Athavale, H. Y. Li and Y. Jiang (2002). Mathematical basis and validation of the full cavitation model. *Journal of Fluids Engineering-Transactions of the ASME* 124, 617–624.

Wu, Y. L., S. H. Liu, H. S. Dou, S. F. Wu and T. J. Chen (2012). Numerical prediction and similarity study of pressure fluctuation in a prototype Kaplan turbine and the model

turbine, *Computers & Fluids* 56, 128–142.

Zhao, Y., G. Y. Wang, B. Huang and Q. Wu (2016). Lagrangian investigations of vortex dynamics in time-dependent cloud cavitating flows, *International Journal of Heat and Mass Transfer* 93, 167–174.

Zhang, Y. L., Y. Li, Z. C. Zhu and B. L. Cui (2014). Computational analysis of centrifugal pump delivering solid-liquid two-phase flow during startup period. *Chinese Journal of Mechanical Engineering* 27(1), 178–185.

Zhou, M. M., H. X. Liu, C. Kang and X. Wei (2019). Resistance of curved surfaces to the cavitation erosion produced through high-pressure submerged waterjet. *Wear* 440, 203091.